Intermediate Yb Valence in the Zintl Phases $Yb_{14}MSb_{11}$ (M = Zn, Mn, Mg): XANES, Magnetism, and Heat Capacity

Allan He[1], Elizabeth L. Kunz Wille[1], Liane M. Moreau[2], Sean M. Thomas[3], Jon M. Lawrence[3], Eric D. Bauer[3], Corwin H. Booth[2]*, Susan M. Kauzlarich*[1]
[1]Department of Chemistry, One Shields Ave, University of California, Davis, CA 95616
[2]Chemical Sciences Division, Lawrence Berkeley National Laboratory, Berkeley, CA 94720
[3]Materials, Physics and Applications Division, Los Alamos National Laboratory, Los Alamos, NM 87545

Corresponding Authors Email: smkauzlarich@ucdavis.edu; chbooth@lbl.gov

Abstract

$Yb_{14}MnSb_{11}$ is a magnetic Zintl compound as well as being one of the best high temperature p-type thermoelectric materials. According to the Zintl formalism, which defines intermetallic phases where cations and anions are valence satisfied, this structure type is nominally made up of 14 Yb^{2+}, 1 $MnSb_4^{9-}$, 1 Sb_3^{7-}, and 4 Sb^{3-} atoms. When Mn is replaced by Mg or Zn, the Zintl defined motifs become 13 Yb^{2+}, 1 Yb^{3+}, 1 (Mg, Zn)Sb_4^{10-}, 1 Sb_3^{7-}, and 4 Sb^{3-}. The predicted existence of Yb^{3+} based on simple electron counting rules of the Zintl formalism calls the Yb valence of these compounds into question. XANES, magnetic susceptibility, and specific heat measurements on single crystals of the three analogs show signatures of intermediate valence Yb behavior and in particular, reveal the heavy fermion nature of $Yb_{14}MgSb_{11}$. In these isostructural compounds, Yb can exhibit a variety of electronic configurations from intermediate (M = Zn), mostly 2+ (M = Mn), to 3+ (M = Mg). In all cases, there is a small amount of intermediate valency at the lowest temperatures. The amount of intermediate valency is constant for M = Mn, Mg and temperature dependent for M = Zn. The evolution of the Yb valence correlated to the transport properties of these phases is highlighted. The presence of Yb in this structure type allows for fine tuning of the carrier concentration and thereby the possibility of optimized thermoelectric properties along with unique magnetic phenomena.

I. INTRODUCTION

The broad class of materials known as Zintl phases are considered charge balanced intermetallic compounds that are composed of cations and polyatomic anions where the oxidation states can be clearly calculated and electrons are considered to be completely transferred from the cations to the anionic units [1]. Among Zintl compounds, many unique and interesting physical properties have been discovered and continue to be uncovered [2-6]. In terms of electronics, Zintl phases are generally semiconducting; however, they can be tuned to be insulating or metallic. Control of electronic behavior for a particular phase is possible because of the large number of possible substitutions that can be accommodated into the structure, in addition to effects stemming from non-stoichiometry and defects. These factors will inherently change density of states near the Fermi level to have a direct effect on the physical properties. The flexibility of electronic tuning in Zintl phases has been utilized among the thermoelectric community where carrier concentrations can be tailored based on Boltzmann transport models to maximize thermoelectric performance [7]. This approach has yielded tremendous success across all temperature regions in such compounds as $Yb_{14}Mn_{1-x}Al_xSb_{11}$ [8], $Ca_{3-x}Na_xAlSb_3$ [9], $Yb_{21-x}Na_xMn_4Sb_{18}$ [10], and $Pb_{1-x}Tl_xTe$ [11]. In particular, $Yb_{14}MSb_{11}$ (M = Mn, Mg) are among the best p-type high temperature thermoelectrics [12-14]. This is attributed to their stability at high temperature (>1273 K), along with a reasonable Seebeck coefficient, electrical resistivity and very low thermal conductivity.

The $A_{14}MPn_{11}$ (14-1-11) structure type [15] (tetragonal $I4_1/acd$) is comprised of an alkaline earth or rare earth atom on the A sites, a transition metal, alkaline earth, or triel on the M site, and pnictogen on the Pn sites. Aside from the high thermoelectric performance, this structure type exhibits a whole range of magnetic and electronic behavior: ferromagnetism [16], antiferromagnetism [17], CMR [16,17], being close to half-metallic [18], as well as being a rare underscreened Kondo system [19]. According to the Zintl formalism for $Yb_{14}MnSb_{11}$ (**Figure 1**),

this structure type is nominally made up of 14 Yb^{2+}, 1 $MnSb_4^{9-}$, 1 Sb_3^{7-}, and 4 Sb^{3-} atoms with 8 formula units per unit cell.

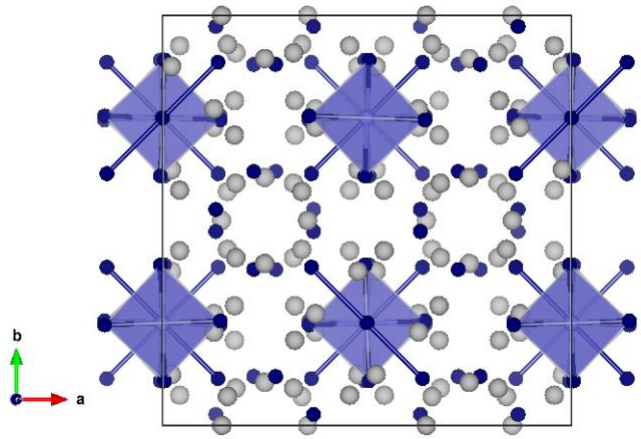

Figure 1. (Color online) Crystal structure of $Yb_{14}MnSb_{11}$ viewed down the *c*-axis (a = 16.578 Å, c = 21.897 Å, tetragonal space group, $I4_1/acd$). Yb atoms are shown in light gray, Mn atoms in light blue, and Sb atoms in navy.

The magnetic behavior of $Yb_{14}MnSb_{11}$ was initially investigated by Fisher et al. [20], and described as consistent with Mn^{3+} (d^4), showing no evidence of Yb^{3+} (f^{13}) from Curie-Weiss law fitting and therefore Yb oxidation state was assigned as Yb^{2+} (f^{14}, nonmagnetic). Subsequent X-ray magnetic circular dichroism (XMCD) studies [21] on single crystals revealed a strong dichroism signal at the Mn $L_{2,3}$–edge that is better described as Mn^{2+} (d^5) than the Mn^{3+} (d^4) determined from magnetism. Additionally, a dichroism signal anti-aligned with the Mn was observed at the Sb $M_{4,5}$–edge with no evidence of any moment on Yb at the Yb $N_{4,5}$–edge (oxidation state of Yb^{2+} in $Yb_{14}MnSb_{11}$ also confirmed through XPS [22]). These results, taken together with the magnetic data, provide a model where the configuration of the $MnSb_4^{9-}$ cluster is more accurately considered as Mn^{2+} (d^5) + h^+ (a polarized hole carrier (h^+) decentralized over the 4 Sb atoms in the cluster and a moment anti-aligned with the Mn moment), instead of simply Mn^{3+} (d^4). Detailed LSDA calculations on isostructural $(Ca,Ba)_{14}MnBi_{11}$ support this configuration hypothesis [18] where the Mn was calculated to be 2+ with an anti-aligned moment

located on the pnictogen *p* states that participate within the tetrahedra, consistent with the XMCD study [21] and reported magnetism [20]. A recent polarized neutron diffraction study has shown that the picture is more complicated, with the compensating moments not localized on the Sb atoms bonded to Mn in the $MnSb_4^{9-}$ tetrahedra but are distributed fairly uniformly across the unit cell on both Sb and Yb sites [23]. This work provides evidence for the Kondo screening cloud that has been proposed for this compound [19,23].

In contrast to the Mn analog, the Zn and Mg phases of 14-1-11 require from the Zintl formalism the following structural motifs: 13 Yb^{2+}, 1 Yb^{3+}, 1 $(Zn,Mg)Sb_4^{10-}$, 1 Sb_3^{7-}, and 4 Sb^{3-}. The predicted existence of Yb^{3+} based on these simple electron counting rules is confirmed through magnetization measurements on single crystal samples. An effective magnetic moment of μ_{eff} = 3.8 μ_B/fu (fu = formula unit) for T > 150 K is observed for the Zn analog [24] and a μ_{eff} = 3.4 μ_B/fu for the Mg analog [25] suggesting intermediate Yb valence states (Yb^{3+} (f^{13}, J = 7/2) has μ_{eff} = 4.54 μ_B). This hypothesis has been supported through X-ray photoemission spectroscopy (XPS) where both Yb^{2+} and Yb^{3+} have been observed for the Zn analog [22]. Note that a single Yb^{3+} atom per formula unit is not allowed in the 14-1-11 structure since the minimum multiplicity of equivalent sites is two for the A element [15]. Therefore, as a Zintl phase, it is possible that there is an intermediate valency or mixed valency, especially as the *f* level of Yb is expected to be close to the Fermi level and there is covalent/metallic bonding [18,26]. Intermediate valence states generally arise from hybridization of localized d or f electrons with the conduction electrons. The f electrons in systems containing for example, Yb, Eu, or Ce, often fluctuate between two electronic configurations that compete for stability and this is referred to as intermediate valency, whereas mixed valency is a term used when the atom can be assigned a specific integral valence such as 2+ or 3+. While intermediate valency is known in intermetallic compounds [27-32], such

behavior in Zintl phases which are typically semiconductors is rare. In particular, the Yb compounds studied in this work compete between the magnetic $4f^{13}$ state and the non-magnetic $4f^{14}$ state.

Studies of RE^{3+} substitutions into this structure type, $A_{14-x}RE_xMSb_{11}$ show $x = 1$ when A = Ca^{2+} and $x \leq 0.5$ when A = Yb, regardless of the identify of M [33-37]. In all cases, the RE^{3+} is found on more than 1 of the 4 possible crystallographic sites, correlated with size. Overall, in the series of compounds, $Yb_{14}MSb_{11}$ (M = Zn, Mn, Mg), the unit cell increases in the order Zn < Mn < Mg concurrent with the room temperature carrier concentration decreasing with Zn > 1 x 10^{21} cm^{-3}, Mn ≈ 1 x 10^{21} cm^{-3}, and Mg ≈ 5 x 10^{20} cm^{-3} [12,13,38,39]. For these compounds, the Zn analog is too metallic for good thermoelectric properties but both the M = Mn, Mg phases are excellent high temperature p-type thermoelectrics [12-14]. A recent paper showed that adding a small amount of RE^{3+} to $Yb_{14}ZnSb_{11}$ dramatically increased the thermoelectric efficiency [37]. Because of the important role of Yb valence in these compounds and the possibility of a localized Yb^{3+} (J = 7/2) heavy fermion state for $Yb_{14}MgSb_{11}$, XANES, magnetic susceptibility, and heat capacity measurements on single crystals of the three analogs were performed. The contribution of Yb to properties of these systems is elucidated providing insight that may be also applied to other Yb containing Zintl phases with an aim towards optimized thermoelectric properties along with new and unique physics.

II. EXPERIMENTAL DETAILS

Synthesis: The single crystals of $Yb_{14}MSb_{11}$ were synthesized through previously reported flux methods [20,24,25]. The crystals were approximately 2 x 2 x 2 mm^3 in dimensions with highly reflective facets (see **Supplemental Material Figure S1** [40]).

XANES Measurements: X-ray absorption near-edge structure (XANES) data were collected on beamline 11-2 at the Stanford Synchrotron Radiation Lightsource using a half-tuned Si(220)

double-crystal monochromator ($\phi = 0°$). Single crystal samples were placed into a slotted aluminum sample holder which was then put into a liquid helium flow cryostat. Yb L_{III}-edge data were collected in fluorescence mode at 4 different temperatures: 20 K, 100 K, 200 K and 300 K. Data were corrected for the dead time of the 100-element germanium detector and a constant background was fit to the lowest-energy data in each scan and subtracted from the data. The incident energy was calibrated by setting the peak in the first derivative of the absorption spectrum of a Yb_2O_3 sample to 8943.0 eV. The data were corrected for self absorption using the FLUO program [41], and the results were also normalized to the data above the edge.

Magnetic Susceptibility and Specific Heat Measurements: The magnetic susceptibility measurements were performed in a SQUID magnetometer from 2 – 300 K in a magnetic field (0.01 T for M = Mn, 1 T for M = Mg, 0.1 T for M = Zn). The data for M = Mn, Zn, Mg were collected as previously described and in the case of M = Mn, Zn, with the easy axis (*c* axis) aligned parallel to the field [24,25,42]. Since M = Mg showed paramagnetic behavior regardless of orientation, no efforts were made to align the crystal with regards to the applied magnetic field. The specific heat for M = Mg was measured from 0.4 – 300 K using a thermal relaxation method (0 T – 1 T).

III. RESULTS & DISCUSSION

Figure 2a compares XANES spectra collected at 20 K for the three compounds $Yb_{14}MSb_{11}$ (M = Mn, Mg, Zn), together with the spectrum from a Yb_2O_3 standard as a benchmark for the Yb^{3+} peak. All three compounds have a dominant peak at about 8939 eV (8 eV below that of Yb_2O_3), indicative of a predominantly Yb(II) configuration. A shoulder at 8947 eV, consistent with the main peak energy of Yb_2O_3 indicates a relatively small amount of 3+ character that is somewhat more pronounced in $Yb_{14}MgSb_{11}$. $Yb_{14}MnSb_{11}$ has the lowest fraction of 3+, as is also visually observed in having the lowest shoulder. Still, there appears to be an unexpectedly high 3+ fraction even for this sample. A FEFF [43] calculation confirms that this shoulder is not due to an EXAFS

oscillation. **Figure 2b** displays temperature-dependent behavior of the $Yb_{14}ZnSb_{11}$ XANES data. At 20 K, the Zn sample spectrum appears similar to that of the Mn and Mg samples; however, increasing temperature results in a decrease in the 2+ peak amplitude at lower energy and an increase in the 3+ peak at higher energy. Spectra collected at other temperatures for $Yb_{14}MnSb_{11}$ and $Yb_{14}MgSb_{11}$ (see **Supplemental Material Figure S2** [40]) are nearly identical and indicate no significant temperature dependence with regards to the Yb valence.

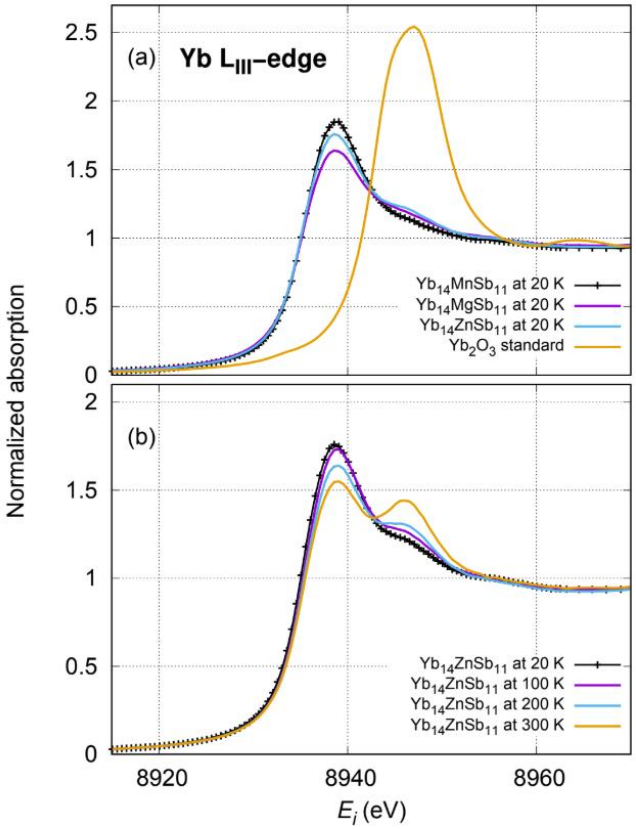

Figure 2. (Color online) **(a)** XANES spectra of the three analogs of $Yb_{14}MSb_{11}$ (M = Zn, Mn, Mg,) collected at 20 K at the Yb L_{III} edge along with a Yb_2O_3 standard. **(b)** Temperature dependence of $Yb_{14}ZnSb_{11}$ showing the increase of the Yb^{3+} peak with increasing T.

Figure 3a shows the fit to the XANES spectrum of the $Yb_{14}ZnSb_{11}$ compound at 20 K. Fits for $Yb_{14}ZnSb_{11}$ at other temperatures and 20 K fits for M = Mn, Mg can be found in **Supplemental Material** (**Figure S3** [40]). The relative $2^+/3^+$ character of Yb is based on the relative peak ratios at the Yb-L_{III} absorption edge. In order to extract an estimate of the Yb valence, we fit the spectra

using a previous method [44,45] that utilizes a broadened arctan-like function [46] (actually an integrated Gaussian) to account for transitions to the continuum (dashed, purple). A Gaussian profile is used to describe the main peak associated with the Yb(II) configuration, another to describe the Yb(III) configuration, and another to model the first structural oscillation. Note that Gaussians are used rather than Lorentzian or pseudo-Voigt profiles since all of these profiles are to represent a collection of discrete transitions, e.g. the two continuum functions associated with the Yb(II) and Yb(III) configurations, or the crystal field-split 5d manifold that accounts for part of the width of the individual configuration peaks. The widths of the individual configuration peaks are held equal, and the position of the arctan-like function is set to the weighted mean position of the configuration peaks. The structural oscillation is due to the Extended X-ray Absorption Fine Structure (EXAFS), which occurs from backscattering of the photoelectron off neighboring atoms [43] and is only included to account for any overlap with the Yb(III) peak. This weighted sum of the peak areas of the individual configuration peaks gives an f-hole occupancy, $n_{f,avg} = A_{Yb(III)}/(A_{Yb(II)}+A_{Yb(III)})$, where a given $n_{f,avg} = 0$ denotes a full-shell, divalent, f^{14} configuration, and $n_{f,avg} = 1$ denotes a trivalent, f^{13} configuration ($J = 7/2$). The overall resulting fits (red) overlay well with the experimental data (black).

At 20 K, the $Yb_{14}MSb_{11}$ compounds each have a similar valence state for the Yb, with $n_{f,avg}$ = 0.27(2), 0.23(2), and 0.28(3) for M = Zn, Mn, and Mg, respectively. The temperature dependence of $n_{f,avg}$ for M = Zn is shown in **Figure 3b**, increasing monotonically from about 0.27(2) to 0.39(1).

Fisher et al. [24] make the point that it is simplistic to treat $Yb_{14}ZnSb_{11}$ as having integral valence on each Yb site because covalent or metallic bonding is undoubtedly present. Based on the susceptibility and specific heat, they conclude that for $Yb_{14}ZnSb_{11}$ a small fraction of the Yb atoms are intermediate valent. The results reported here show that the Yb atoms are not all divalent

in any of the three analogs. The measurements provide the average valence of Yb and the specific valence on the four inequivalent Yb sites in the crystal structure cannot be deconvoluted. It is clear, however, that for all three compounds, the Yb atoms are on the whole strongly intermediate-valent with a mean occupation number of approximately $n_{f,avg} \approx 0.25$ at T = 20 K from XANES. It is therefore more accurate to consider the bonding in this structure type to be covalent/metallic in character with some contribution or hybridization from the Yb 4f electrons with the Sb p states. It is also likely that the availability (or lack thereof) of *d* orbitals on M (Zn, d^{10}, Mn, d^5, Mg, d^0) contribute to the hybridization. The situation is reminiscent of that for CeO_2, which formally would have tetravalent cerium; in reality the cerium atoms have strong intermediate valence [47,48]. Previous studies of XMCD [21] and XPS [22] could not definitively determine the bulk Yb^{3+} contribution to these systems because of the difference in energy between the techniques.

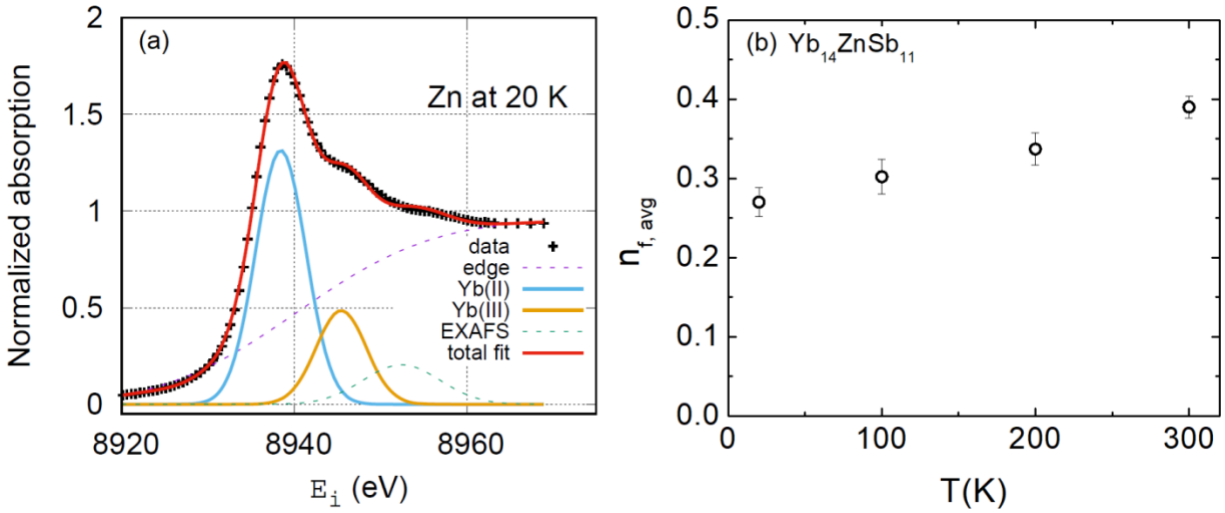

Figure 3. (Color online) **(a)** XANES fitting and extraction of the 3+ fraction in the $Yb_{14}ZnSb_{11}$ sample at 20K. **(b)** Temperature dependence of $n_{f,avg}$ for the $Yb_{14}ZnSb_{11}$ sample.

Magnetic susceptibility of the three compounds are shown in **Figure 4** and specific heat in **Figure 5**. The units are given in terms of mole-formula-units (mol-fu) so that each plot represents the contribution of the 14 Yb atoms. Strongly intermediate valent compounds occur when there is

substantial hybridization between the 4f electrons and the ligand electrons. The characteristic (Kondo) energy for 4f excitations in these compounds is typically very large ($T_K >> 1000$ K) which leads to a small contribution to the linear coefficient of specific heat ($\gamma \approx 1/T_K < 10$ mJ/mol-K^2) and small Pauli susceptibility ($\chi_p \approx 1/T_K < 10^{-3}$ emu/mol). The susceptibility and 4f occupation number vary on the scale of the Kondo temperature so for such a large T_K, both n_f and χ will exhibit very little change below room temperature [49,50].

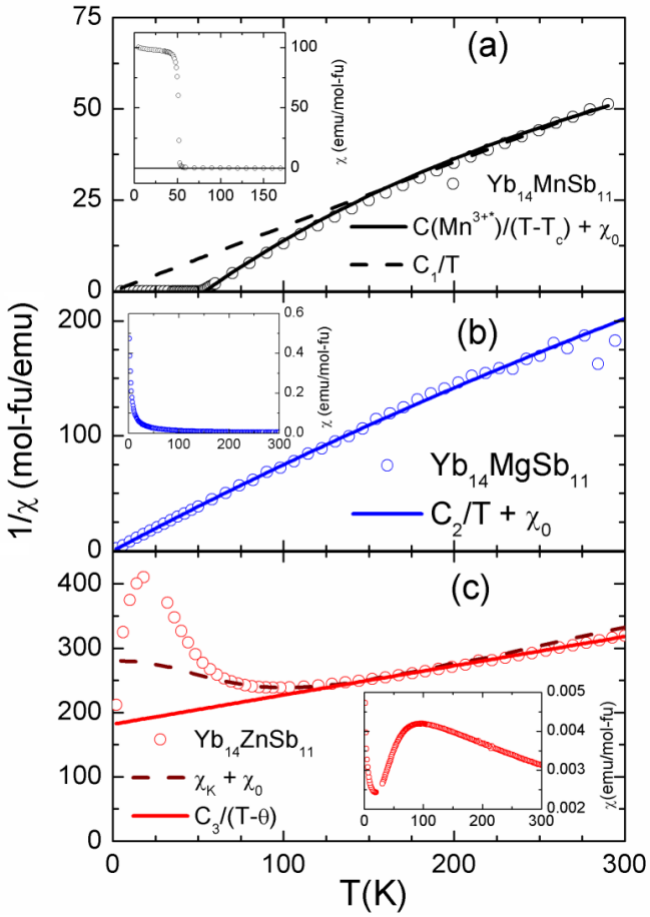

Figure 4. (Color online) The inverse susceptibility $\chi(T)^{-1}$ of the three $Yb_{14}MSb_{11}$ (M = Mn, Mg, Zn) compounds (the formulae given for the dashed and solid lines are direct susceptibility $\chi(T)$ which are also included as insets) between 2 and 300 K. **(a)** $Yb_{14}MnSb_{11}$ **(b)** $Yb_{14}MgSb_{11}$ **(c)** $Yb_{14}ZnSb_{11}$. The dashed and solid lines are not least squares fits but give comparisons of the data to the formulae. These serve the purpose of showing how our data favorably compares to other groups and allow us to make reasonable estimates of the Mn and Yb moments, as well as the fraction of Yb^{3+} involved.

Consider first the case of $Yb_{14}MnSb_{11}$. The ferromagnetic transition at $T_c \approx 54$ K is clearly observed in the magnetic susceptibility as displayed in the inset to **Figure 4a**. The Curie constant associated with the $\chi(T) = C/(T - T_c) + \chi_0$ fit in **Figure 4a** is associated with a Mn^{3+*} (d^4) (where $Mn^{3+*} = Mn^{2+}$ (d^5) + h^+, S = 4/2) configuration. These results are in excellent agreement with those reported in Ref. [20], albeit that the constant term $\chi_0 = 7.0 \times 10^{-3}$ emu/mol-fu is slightly larger than the value 4.9×10^{-3} emu/mol-fu reported there. Above 200 K, the data can be approximated by a simple Curie law $\chi(T) = C_1/T$ where $C_1 = 5.65$ emu-K/mol-fu ($\mu_{eff} = 6.72\ \mu_B$/fu). This is considerably larger than the value C = 3.00 emu-K/mol-fu ($\mu_{eff} = 4.90\ \mu_B$/fu) expected for a Mn^{3+*} configuration with L = 0 and g = 2 or even Mn^{2+} (C = 4.38 emu-K/mol-fu; $\mu_{eff} = 5.92\ \mu_B$/fu). Assuming that the Mn stays 2+ to high T, the difference between the high T Curie constant (C = 5.65 emu-K/mol-fu, $\mu_{eff} = 6.72\ \mu_B$/fu) and the Mn^{2+} moment is C = 1.27 emu-K/mol-fu ($\mu_{eff} = 3.19\ \mu_B$/fu) which is half the value of $C_{7/2} = 2.58$ emu-K/mol-Yb ($\mu_{eff} = 4.54\ \mu_B$/Yb) expected for the single Yb^{3+} ($J = 7/2$) local moment. This analysis ignores any potential constant term, which would reduce the Curie constant. Given the downward curvature in the inverse susceptibility of this compound, the high T Curie constant is potentially even larger. Despite these caveats, it makes sense that in the paramagnetic region the Yb might contribute to the high temperature Curie constant with a magnitude similar to that seen in the M = Mg compound, see below.

The susceptibility of $Yb_{14}MgSb_{11}$ (**Figure 4b**) is well described by a Curie law with a small constant term $\chi(T) = C_2/T + \chi_0$ where $C_2 = 1.26$ emu-K/mol-fu ($\mu_{eff} = 3.17\ \mu_B$/fu) is again about half the value expected for a single Yb^{3+} ($J = 7/2$, $C_{7/2} = 2.58$ emu-K/mol-Yb, $\mu_{eff} = 4.54\ \mu_B$/fu) local moment in the formula unit and χ_0 is an order of magnitude smaller ($\chi_0 = 7.5 \times 10^{-4}$ emu/mol-fu) than the constant contribution used in fitting the Mn compound. The fitting of the Mg analog is essentially identical to that reported in Ref. 25, where the data from 50 – 250 K was fit to a

Curie-Weiss law $\chi = C_2/(T - \theta)$ and obtained $C_2 = 1.46$ emu-K/mol-fu and $\theta = 3.6$ K [25]. Wille et al. [25] have shown via X-ray diffraction that there are Mg atoms on the Yb(1) and/or Yb(3) sites in the single crystal sample. The appropriate stoichiometry was found to be $(Yb_{13.8}Mg_{0.2})MgSb_{11}$ which was confirmed by electron microprobe measurements. The Curie-law susceptibility seen in this compound is attributed to approximately a single Yb^{3+} atom in the formula unit. As indicated above in the Introduction, the existence of one trivalent Yb atom per formula unit cannot be explained if the material possesses perfect structural order, but it could arise from site disorder. Yb atoms in a disordered environment can experience a weaker-than-average 4f/conduction hybridization, and hence can be trivalent. An active (trivalent) Yb site number of precisely one could also occur if there were a modification of the $Ca_{14}AlSb_{11}$-structure type removing the equivalency of the atoms on one of the Yb sites; however, such a modified structure has not been observed to date.

Under the assumption that there are 13 Yb_A atoms, all with identical strong intermediate valence, and one active Yb_B atom per formula unit, we can use **Equation 1**:

$$\frac{13n_{f,A}(Yb_A) + n_{f,B}(Yb_B)}{14} = n_{f,avg} \qquad \textbf{(Equation 1)}$$

For a $n_{f,avg} = 0.28$ and $n_{f,B} = 1$, we obtain $n_{f,A} = 0.224$ for $Yb_{14}MgSb_{11}$. Hence the existence of one trivalent Yb atom has only a small effect on the average valence of the other sites, but also leads to no temperature dependence for n_f, as observed, since the atom will remain trivalent to high temperature.

The fact that the Curie constant (**Figure 4b**) is only half that expected for a Yb^{3+} ($J = 7/2$) moment could arise from crystal field (CF) splitting. The small constant contribution $\chi_0 = 7.5\text{x}10^{-4}$ emu/mol-fu could easily arise from the other 13 strongly intermediate valent Yb's, each

contributing $\chi_p \approx 6x10^{-5}$ emu/mol-fu. The CF splitting, however, would have to be much greater than 30 meV in order to give a Curie law behavior below 300 K in a pure doublet CF ground state. For smaller CF energies, the contributions from the gradual excitation of higher-lying crystal field multiplets would lead to deviations from the Curie law below room temperature. We note that such a large CF splitting is unusual for Yb where simple Curie behavior is rarely observed over the whole interval 2 – 300 K.

The high temperature susceptibility of $Yb_{14}ZnSb_{11}$ approximately follows a Curie-Weiss law with a value $C_3 = 2.2$ emu-K/mol-fu ($\mu_{eff} = 4.19\ \mu_B$/fu) that is slightly smaller than $C_{7/2}$; the value of θ is -400 K (solid line in **Figure 4c**). This behavior is typical of Yb intermediate valence compounds [49,50] whose susceptibility often can be described by that calculated for a Kondo impurity. The dashed line in **Figure 4c** gives the result of such a calculation [51] with $T_K = 450$ K, put on an absolute basis by utilizing the formula $\chi_K(0) = (2J+1)/2\pi)*C_J/T_K$ for the zero temperature susceptibility; the Curie constant is that of a single Yb^{3+} ($J = 7/2$) local moment in the formula unit. The Kondo curves given here are strictly valid only in the Kondo limit $n_f \rightarrow 1$, i.e when the Yb is close to trivalent. Inclusion of a small constant term, identical to that of $Yb_{14}MgSb_{11}$, brings the theory curve into excellent alignment with the data. These data are again in good agreement with those reported earlier [24]. Although there has been no report for this compound of the kind of site disorder seen in $Yb_{14}MgSb_{11}$, we assume that such disorder is present and leads to a moderately weak hybridization on the approximately one active Yb site per formula unit than on the other 13 sites. Such a moderate hybridization would then cause the Kondo effect with the value $T_K \approx 450$ K observed for this compound.

It can be seen in **Figure 5a** that the total specific heats C(T) of all three compounds are nearly equal over the interval 2 – 300 K. This implies that the phonons, which make the major

contribution to the total specific heat, are essentially identical in all three materials [52]. In **Figure 5b** we compare the low temperature behavior of C/T for the Mn and Zn compounds to the form $C/T = \gamma + AT^2$. The coefficient of the phonon term is indeed identical for both materials, and the Sommerfeld coefficients (γ) are in reasonable agreement with those reported earlier. For the Mn compound, Ref. [19] found $\gamma = 160$ mJ/mol-fu-K^2, Ref. [20] found $\gamma = 70$ mJ/mol-fu-K^2, and Ref. [53] found $\gamma = 145$ mJ/mol-fu-K^2, which compare to our value 125 mJ/mol-fu-K^2. Our XANES results show that the Yb atoms are on average strongly intermediate valent with $n_{f,avg} = 0.23(2)$ and no detectable temperature dependence of $n_{f,avg}$. The small constant term in the susceptibility and the linear coefficient of specific heat may be properties of the ordered phase [20], and possibly include a contribution from the 14 strongly intermediate valent Yb atoms. For the Zn compound, Ref. [24] found a value 80 mJ/mol-fu-K^2, close to our value $\gamma = 55$ mJ/mol-fu-K^2. While the linear coefficient of specific heat is affected by the ferromagnetism for M = Mn, that for the M = Zn compound is typical of moderately intermediate valent materials. For the Mg analog, the low temperature data show a peak in C/T near $T_{max} = 0.7$ K with a magnitude 2.17 J/mol-fu-K^2 (**Figure 5b**). Such a large value of C/T is characteristic of extremely heavy fermion and/or magnetic order. The origin of the maximum is discussed below.

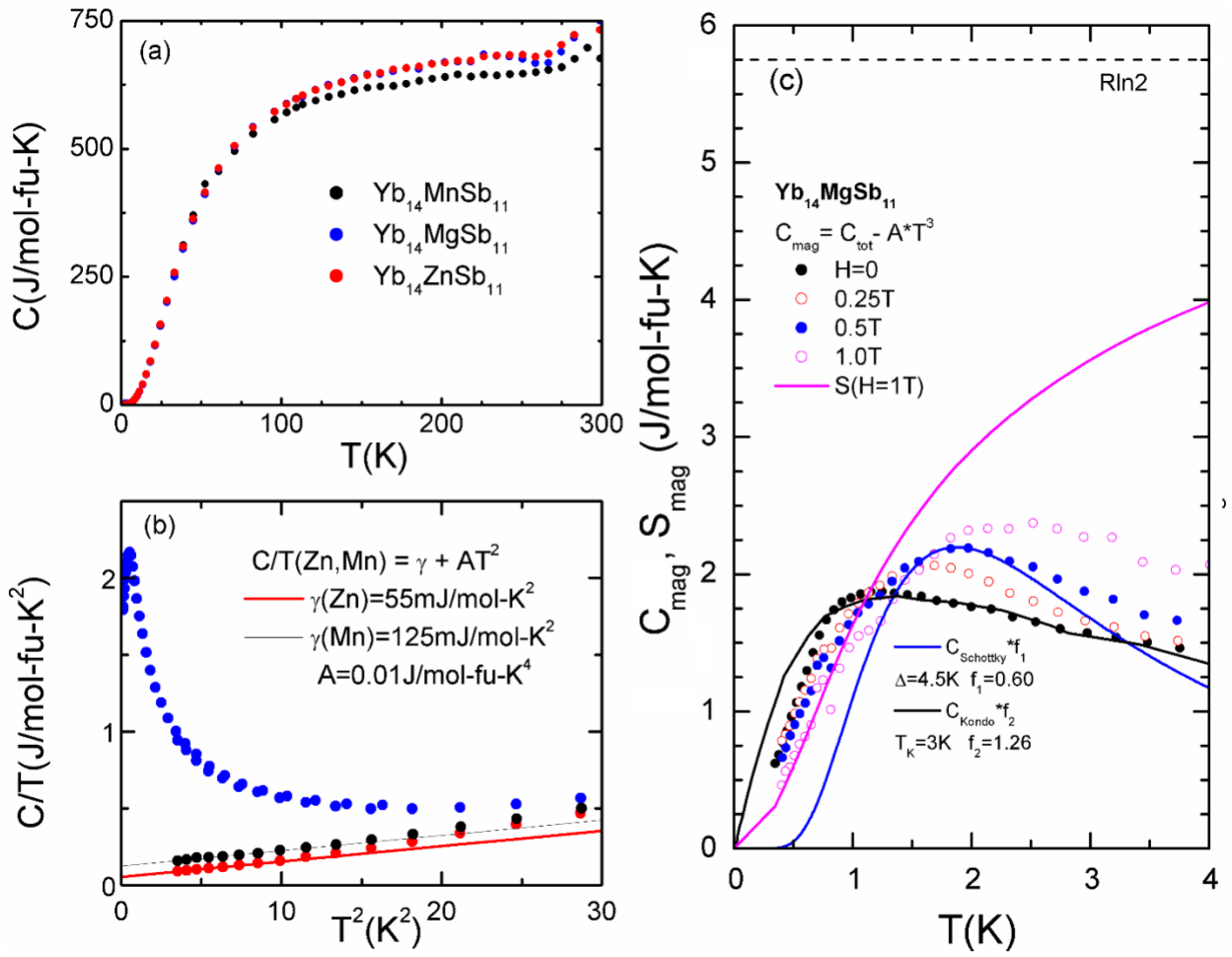

Figure 5. (Color online) The specific heat C(T) of all three $Yb_{14}MSb_{11}$ (M = Mn, Mg, Zn) compounds. **(a)** C(T) plotted over the temperature range 2 - 300K. **(b)** The low temperature specific heat with the same legend for the data as in **(a)** divided by the temperature, C(T)/T. The maximum at T = 0.7K for M = Mg is typical of very heavy fermion behavior and/or magnetic order. **(c)** The specific heat of $Yb_{14}MgSb_{11}$ for four magnetic fields in the range 0 - 1T and temperature in the range 0.3 – 4 K. The black line is the theoretical Kondo curve [51] for J = 1/2, T_K = 3 K, and for 1.26 Yb^{3+} atoms per fu. The blue line is the Schottky specific heat for a two-level (J = 1/2) system with splitting Δ = 4.5K and for 0.6 Yb^{3+} per fu. The magenta line is the magnetic entropy for H = 1T.

Figure 5c shows the specific heat for $Yb_{14}MgSb_{11}$ in the range 0.3 – 4 K and for $0 < H < 1$T. Subtracting the phonon term AT^3 with the same value of A as observed in the Mn and Zn compounds, we determine the magnetic contribution to the specific heat of $Yb_{14}MgSb_{11}$, which is peaked at temperatures that increase with H. The data follow closely the predictions [51] for 1.26 Kondo doublets in the formula unit with T_K = 3 K (black line, **Figure 5c**). Kondo doublet ground states typically occur in heavy fermion compounds where the crystal field splitting of the Yb J =

7/2 multiplet is much larger than the Kondo temperature, and such low-T_K compounds are always very close to trivalent. The small-T_K Kondo behavior for this compound would then arise from weaker-than-average hybridization of the Yb^{3+} 4f doublets with the conduction electrons. Also, as can be seen for the $H = 0.5$ T data with the blue line **Figure 5c**, the peaks in C(T) are broader than expected for a two-level ($J = 1/2$) Schottky doublet. The entropy (which we show for $H = 1$ T) appears to be approaching the value Rln2 as the temperature is raised to 9 K (not shown), suggesting that the peak represents the contribution of a ground state Yb crystal field doublet.

It is possible that the peaks in C(T) seen for $Yb_{14}MgSb_{11}$ in the range $0 < H < 1$T arise from magnetic order, where the disorder in the system creates a broadening beyond that expected for a clean system. If this is the case, then the peak near 0.7 K at $H = 0$ would arise from a broadened phase transition, and the peaks at higher temperature as the field is raised would reflect Zeeman splitting of the ground state doublets. We note, however, that entropy at the peak in C/T for $H = 0$ is less than 1 J/mol-fu-K. This entropy is such a small fraction of Rln2 that it casts doubt on the interpretation that there is a magnetic phase transition at 0.7 K. In any case, given the disorder, it is not possible at present to distinguish the Kondo mechanism from one of magnetic order. Quite possibly, both the Kondo effect and magnetic correlations are present.

The susceptibility and specific heat of $Yb_{14}ZnSb_{11}$ are typical of moderately intermediate valent compounds, where a maximum in the susceptibility occurs at a temperature $T_{max} = T_K/\alpha$ ($\alpha \approx 3$-5) and the specific heat coefficient is in the range 40 - 100 mJ/mol-fu-K^2. The behavior of $Yb_{14}ZnSb_{11}$ is similar to that of the intermediate valent compound $YbAl_3$ [54], which has a Kondo temperature of nearly 600 K, a maximum in the susceptibility at $T_{max} = 125$ K, and a coefficient of specific heat $\gamma \approx 40$ mJ/mol-K^2. The ground state valence of $YbAl_3$ is of order 2.75 ($n_{f,avg} = 0.75$). It is very likely that the occupation number of the active Yb site in $Yb_{14}ZnSb_{11}$ is similar to this

value. The overall behavior of these intermediate valent 14-1-11 compounds is close to that of a trivalent Kondo theory at high T, but with some differences, especially at low temperature. The deviation of the measured susceptibility from the Kondo curve below 50 K (**Figure 4c**) can be explained from the ratio $\chi(T=0)/\chi(T_{max})$, which is smaller for moderate intermediate valence systems than for trivalent Kondo behavior. The universal (Wilson) ratio between $\chi(0)$ and γ is also altered. For the Zn compound, with T_K = 450 K, the specific heat coefficient in the Kondo limit [51] would be $\gamma = J\pi R/3T_K$ (where R is the gas constant) which for J = 7/2 and T_K = 450 K would give γ = 67 mJ/mol-Yb-K^2 (i.e., one active Yb site), somewhat larger than the value 55 mJ/mol-fu-K^2 (equivalent mJ/mol-Yb-K^2 for 1 Yb) to that we report here.

The occupation numbers of intermediate valent compounds such as $YbAl_3$ increase as the temperature is raised, by an amount $n_{f,avg}(300K) - n_{f,avg}(0K) \approx 0.1 - 0.2$. If in $Yb_{14}ZnSb_{11}$ we assume that the ground state valence of the one active site per fu is $n_f(B) = 0.75$, as for $YbAl_3$, then using **Equation 1** with $n_{f,avg} = 0.27$, we find that $n_f(A) = 0.233$. (We note in passing that the A-site occupations derived in this manner appear to be very similar – of order 0.22-0.23 in all three $Yb_{14}MSb_{11}$ compounds). If the valence of the active site then increases to $n_f(B) = 1$ at 300 K, while the occupation of the other sites stay the same, the resulting average valence at 300 K would be only $n_{f,avg} = 0.288$, not the 0.390 observed for $Yb_{14}ZnSb_{11}$ (**Figure 3b**). This implies that there must be a change in occupation number on the other Yb sites. For example, if the active site occupation number increased to 1 while that of all the other 13 sites increased to 0.343, then an average occupation 0.390 would be observed at 300 K. In other words, the change in $n_{f,avg}$ observed in $Yb_{14}ZnSb_{11}$ is too large to be attributed to merely the one active Yb site per fu, suggesting that some of the other 13 Yb sites exhibit an appreciable increase with temperature. If this involvement of other Yb sites is the case, it is not clear why such an increase is not also observed in $Yb_{14}MnSb_{11}$

and $Yb_{14}MgSb_{11}$, which have comparable average valence at low temperature. However, it has been noted that $Yb_{14}ZnSb_{11}$ has both the smallest unit cell and highest metallic character [20,24,25]. Perhaps the change of valence on the active Yb site feeds back to increase the f-hole content on the inactive sites. Chemical pressure arising from the change in volume associated with the change in valence on the active site is one possible way the observed valence change with temperature might happen.

The hybridization of the Yb 4f states with the p states of the Sb in the valence band is crucial for the intermediate valent nature of the Yb atoms in this system. The relatively low values of $n_{f,avg}$ for all analogs show that the Yb atoms naturally favor the divalent state where the electron is localized on the site, rather than being in the conduction band. The intermediate valency of these systems lends itself to the flexibility of doping for this structure. Substitutions that increase the unit cell volume are expected to decrease the average Yb valence since Yb^{2+} is larger than Yb^{3+}. It is also possible to introduce chemical pressure in the system by formation of a solid solution, which will in turn cause a shift in the average valence state for the Yb. Control of the valence can, in theory, be exploited to enhance the Seebeck coefficient especially since the 4f Yb energy levels fall very close to the Fermi level and increase the figure of merit, zT. Any substitutions or doping into the system will change the degree of intermediate valency on the Yb atoms (as exemplified by the difference between the M = Zn, Mn, Mg) and will simultaneously change the density of states near the Fermi level, as well as the carrier concentration within the system. The difference in the local environment of the Yb atoms due to the valence fluctuations also helps to explain the low thermal conductivity in the 14-1-11 system, where the different environments lead to increased phonon scattering. The idea of exploiting the intermediate valent nature of the rare earth element

has been visited in some skutterudite systems [55,56]. One can expect that there will be an optimal average Yb valence for 14-1-11 to yield the best thermoelectric properties.

IV. CONCLUSIONS

The Yb atoms of the three analogs of $Yb_{14}MSb_{11}$ (M = Zn, Mn, Mg) have been found to exhibit intermediate valence. XANES measurements reveal that while the $Yb_{14}MnSb_{11}$ and $Yb_{14}MgSb_{11}$ analogs have a nearly constant average Yb^{3+} fraction (n_f), $Yb_{14}ZnSb_{11}$ has a $n_{f,avg}$ that is strongly temperature dependent. Using field dependent specific heat measurements, the Mg analog is confirmed to exhibit a Schottky-like anomaly with a peak at T = 0.7 K, consistent with this compound being a heavy fermion. A $n_{f,avg} \approx 0.25$ ($4f^{13.75}$) may be a criterion for the requirements of the Yb containing 14-1-11 structure type.

If we bring these conclusions back to the ideas of employing Zintl formalism for these compounds, it is clear that Yb is close to 2+ in all cases. Since the transport properties of all three are those of a heavily degenerate semiconductor or metal, it suggests that the Yb may be hybridized to give rise to a f electron-count a little less than 14. Since one Yb^{3+} is not allowed given the 2-fold or 4-fold equivalency of the Yb sites, but because the Zintl formulism requires one (for M = Mg, Zn), the compound can accommodate this in one of two ways: (1) create disorder and allow Yb^{3+} on some random sites or (2) undergo a small distortion which allows a one-fold Yb site. Therefore, as the carriers are decreased according to Zn > Mn > Mg, the Zintl formalism is best fulfilled with Mg. These results are consistent with the limited amount of RE^{3+} substitution, $x \leq 0.5$, observed in $Yb_{14-x}RE_xMSb_{11}$, presumably because of the presence of intermediate valence of Yb that also exists in these compounds. Systematic substitution of RE in M = Zn, Mg would provide additional verification of electronic vs size restrictions in this structure type. Systematic synthesis of solid solutions compositions with Yb-Eu and Yb-A (A = alkaline earth) may uncover

quantum behavior in these narrow bandgap semiconductors. Because of the heavy fermion characteristics in $Yb_{14}MgSb_{11}$, replacing Ge for Sb or an alkali metal for Yb, for example, to obtain higher carrier concentrations along with substitution of M with 4d or 5d metals, may result in anomalous behavior induced through hybridization of the Yb 4f orbitals with Sb p and M d orbitals [30]. These results and suggestions for further investigation are relevant to many of the Yb containing Zintl phases with magnetic and thermoelectric properties to consider and may provide a pathway towards quantum behavior and thermoelectric optimization.

Acknowledgements
We thank NSF for funding, DMR-1709382. Work at Lawrence Berkeley National Laboratory was supported by the Director, Office of Science, Office of Basic Energy Sciences, Division of Chemical Sciences, Geosciences, and Biosciences Heavy Element Chemistry Program of the U.S. Department of Energy (DOE) under Contract No. DE-AC02-05CH11231. X-ray absorption measurements were performed at beamline 11-2 at the Stanford Synchrotron Radiation Lightsource, which is supported by the U.S. Department of Energy, Office of Science, Office of Basic Energy Sciences under contract no. DE-AC02-76SF00515. Work at Los Alamos was performed under the auspices of the U.S. DOE, Office of BES, Division of Materials Sciences and Engineering.

References

1. S. M. Kauzlarich, S. R. Brown, G. J. Snyder. Zintl phases for thermoelectric devices. *Dalton Trans.* **2007**, 2099.
2. Y. Hu, G. Cerretti, E. L. K. Wille, S. K. Bux, S. M. Kauzlarich. *J. Solid State Chem.* **2019**, *271*, 88.
3. H. Luo, J. W. Krizan, L. Muechler, N. Haldolaarachchige, T. Klimczuk, W. Xie, M. K. Fuccillo, C. Felser, R. J. Cava. *Nat. Comm.* **2015**, *6*, 6489.
4. W. G. Zeier, J. Schmitt, G. Hautier, U. Aydemir, Z. M. Gibbs, C. Felser, G. J. Snyder. *Nat. Rev. Mater*. **2016**, *1*, 16032.
5. F. Wang, G. J. Miller. *Inorg. Chem.* **2011**, *50*, 7625.
6. A. Ovchinnikov, S. Bobev. *J. Solid State Chem.* **2019**, *270*, 346.
7. E. S. Toberer, A. F. May, G. J. Snyder. *Chem. Mater.* **2010**, *22*, 624.

8. E. S. Toberer, C. A. Cox, S. R. Brown, T. Ikeda, A. F. May, S. M. Kauzlarich, G. J. Snyder. *Adv. Func. Mater*. **2008**, *18*, 2795.
9. A. Zevalkink, E. S. Toberer, W. G. Zeier, E. Flage-Larsen, G. J. Snyder. *Energy Environ. Sci.* **2011**, *4*, 510.
10. A. He, S. K. Bux, Y. Hu, D. Uhl, L. Li, D. Donadio, S. M. Kauzlarich. *Chem. Mater.* **2019**, *31*, 8076.
11. J. P. Heremans, V. Jovovic, E. S. Toberer, A. Saramat, K. Kurosaki, A. Charoenphakdee, S. Yamanaka, G. J. Snyder. *Science*, **2008**, *321*, 554.
12. S. R. Brown, S. M. Kauzlarich, F. Gascoin, G. J. Snyder. *Chem. Mater.* **2006**, *18*, 1873.
13. A. P. Justl, G. Cerretti, S. K. Bux, S. M. Kauzlarich. *J. Appl. Phys.* **2019**, *126*, 165106.
14. Y. Hu, J. Wang, A. Kawamura, K. Kovnir, S. M. Kauzlarich. *Chem. Mater.* **2015**, *27*, 343.
15. G. Cordier, H. Schäfer, M. Stelter. *Z. Anorg. Allg. Chem.* **1984**, *519*, 183.
16. J. Y. Chan, S. M. Kauzlarich, P. Klavins, R. N. Shelton, D. J. Webb. *Chem. Mater.* **1997**, *9*, 3132.
17. J. Y. Chan, S. M. Kauzlarich, P. Klavins, R. N. Shelton, D. J. Webb. *Phys. Rev. B* **1998**, *57*, R8103.
18. D. Sánchez-Portal, R. M. Martin, S. M. Kauzlarich, W. E. Pickett. *Phys. Rev. B* **2002**, *65*, 144414.
19. B. C. Sales, P. Khalifah, T. P. Enck, E. J. Nagler, R. E. Sykora, R. Jin, D. Mandrus. *Phys. Rev. B* **2005**, *72*, 205207.
20. I. R. Fisher, T. A. Wiener, S. L. Bud'ko, P. C. Canfield, J. Y. Chan, S. M. Kauzlarich. *Phys. Rev. B* **1999**, *59*, 13829.
21. A. P. Holm, S. M. Kauzlarich, S. A. Morton, G. D. Waddill, W. E. Pickett, J. G. Tobin. *J. Am. Chem. Soc.* **2002**, *124*, 9894.
22. A. P. Holm, T. C. Ozawa, S. M. Kauzlarich, S. A. Morton, G. D. Waddill, J. G. Tobin. *J. Solid State Chem.* **2005**, *178*, 262.
23. M. B. Stone, V. O. Garlea, B. Gillon, A. Cousson, A. D. Christianson, M. D. Lumsden, S. E. Nagler, D. Mandrus, B. C. Sales. *Phys. Rev. B* **2017**, *95*, 020412.
24. I. R. Fisher, S. L. Bud'ko, C. Song, P. C. Canfield, T. C. Ozawa, S. M. Kauzlarich. *Phys. Rev. Lett.* **2000**, *85*, 1120.
25. E. L. K. Wille, N. H. Jo, J. C. Fettinger, P. C. Canfield, S. M. Kauzlarich. *Chem. Commun.* **2018**, *52*, 12946.
26. H. Kuroiwa, Y. Imai, T. Saso. *J. Phys. Soc. Jpn.* **2007**, *76*, 124704.
27. O. Sichevych, Y. Prots, Y. Utsumi, L. Akselrud, M. Schmidt, U. Burkhardt, M. Coduri, W. Schenelle, M. Bobnar, Y.-T. Wang, Y.-H. Wu, K.-D Tsuei, L. H. Tjeng, Y. Grin. *Inorg. Chem.* **2017**, *56*, 9343.
28. M. Juckel, P. Koželj, Y. Prots, A. Ormeci, U. Burkhardt, A. Leithe-Jasper, E. Svanidze. *Z. Anorg. Allg. Chem.* **2020**, *646*, 1.
29. B. K. Rai, I. W. H. Oswald, J. Y. Chan, E. Morosan. *Phys. Rev. B.* **2016**, *93*, 035101.
30. X. Gui, T.-R. Chang, K. Wei, M. J. Daum, D. E. Grav, R. E. Baumbach, M. Mourigal, W. Xie. *ACS Cent. Sci.* **2020**, DOI: 10.1021/acscentsci.0c00691.
31. S. Nakatsuji, K. Kuga, Y. Machida, T. Tayama, T. Sakakibara, Y. Karaki, H. Ishimoto, S. Yonezawa, Y. Maeno, E. Pearson, G. G. Lonzarich, L. Balicas, H. Lee, Z. Fisk. *Nat. Phys.* **2008**, *4*, 603.
32. R. T. Macaluso, S. Nakatsuji, K. Kuga, E. Thomas, Y. Machida, Y. Maeno, Z. Fisk, J. Y. Chan. *Chem. Mater.* **2007**, *19*, 1918.

33. A. Ovchinnikov, J. Prakash, S. Bobev. *Dalton Trans*. **2017**, *46*, 16041.
34. J. Prakash, S. Stoyko, L. Voss, S. Bobev. *Eur. J. Inorg. Chem.* **2016**, 2016, 2912.
35. Y. Hu, C. –W. Chen, H. Cao, F. Makhmudov, J. H. Grebenkemper, M. N. Abdusalyamova, E. Morosan, S. M. Kauzlarich. *J. Am. Chem. Soc.* **2016**, *138*, 12422.
36. I. G. Vasilyeva, R. E. Nikolaev, M. N. Abdusaljamova, S. M. Kauzlarich. *J. Mater. Chem. C.* **2016**, *4*, 3342.
37. E. L. K. Wille, N. S. Grewal, S. K. Bux, S. M. Kauzlarich. *Materials* **2019**, *12*, 731.
38. J. H. Grebenkemper, Y. Hu, D. Barrett, P. Gogna, C. –K. Huang, S. K. Bux, S. M. Kauzlarich. *Chem. Mater.* **2015**, *27*, 5791.
39. S. R. Brown, E. S. Toberer, T. Ikeda, C. A. Cox, F. Gascoin, S. M. Kauzlarich, G. J. Snyder. *Chem. Mater.* **2008**, *20*, 3412.
40. See Supplemental Material at [URL will be inserted by publisher] for image of typical flux grown crystals, temperature dependent XANES, XANES Fits.
41. D. Haskel. FLUO: Correcting XANES for self absorption in fluorescence measurements. https://www.aps.anl.gov/xfd/people/haskel/fluo.html. **1999.**
42. J. H. Grebenkemper, S. M. Kauzlarich. *APL Mater.* **2015**, *3*, 041503.
43. J. J. Rehr, R. C. Albers. *Rev. Mod. Phys.* **2000**, *72*, 621.
44. C. H. Booth, A. D. Christianson, J. M. Lawrence, L. D. Pham, J. C. Lashley, F. R. Drymiotis. *Phys. Rev. B* **2007**, *75*, 012301.
45. C. H. Booth, M. D. Walter, D. Kazhdan, Y. –J. Hu, W. W. Lukens, E. D. Bauer, L. Maron, O. Eisenstein, R. A. Andersen. *J. Am. Chem. Soc.* **2009**, *131*, 6480.
46. R. L. Halbach, G. Nocton, C. H. Booth, L. Maron, R. A. Andersen. *Inorg. Chem.* **2018**, *57*, 7290.
47. A. Kotani. *Mod. Phys. Lett. B* **2013**, *27*, 1330012.
48. S. G. Minasian, E. R. Batista, C. H. Booth, D. L. Clark, J. M. Keith, S. A. Kozimor, W. W. Lukens, R. L. Martin, D. K. Shuh, S. C. E. Stieber, T. Tylisczcak, X. –D. Wen. *J. Am. Chem. Soc.* **2017**, *139*, 18052.
49. J. Lawrence. *Mod. Phys. Lett.* B **2008**, *22*, 1273.
50. J. M. Lawrence, P. S. Riseborough, R. D. Parks. *Rep. Prog. Phys.* **1981**, *44*, 1.
51. V. T. Rajan. *Phys. Rev. Lett.* **1983**, *51*, 308.
52. R. Hanus, G. Janine, M. Wood, Y. Cheng, D. L. Abernathy, M. E. Manley, G. Hautier, G. J. Snyder, R. Hermann. Transition from Crystal-like to Amorphous-like Heat Conduction in Structurally-Complex Crystals. *ChemRxiv*. **2020**, https://doi.org/10.26434/chemrxiv.12252056.v1
53. K. S. Burch, A. Schafgans, N. P. Butch, T. A. Sayles, M. B. Maple, B. C. Sales, D. Mandrus, D. N. Basov. *Phys. Rev. Lett.* **2005**, *95*, 046401.
54. A. L. Cornelius, J. M. Lawrence, T. Ebihara, P. S. Riseborough, C. H. Booth, M. F. Hundley, P. G. Pagliuso, J. L. Sarrao, J. D. Thompson, M. H. Jung, A. H. Lacerda, G. H. Kwei. *Phys. Rev. Lett.* **2002**, *88*, 117201.
55. G. S. Nolas, D. T. Morelli, T. M. Tritt. *Annu. Rev. Mater. Sci.* **1999**, *29*, 89.
56. E. Bauer, S. Berger, C. Paul, H. Michor, A. Grytsiv, P. Rogl. *Phys. B* **2003**, *328*, 49.

Magnetic susceptibility, specific heat, and XANES measurements on single crystals of the three analogs of $Yb_{14}MSb_{11}$ (M = Mn, Mg, Zn) show intermediate valence Yb behavior and in particular, reveal the heavy fermion nature of $Yb_{14}MgSb_{11}$.

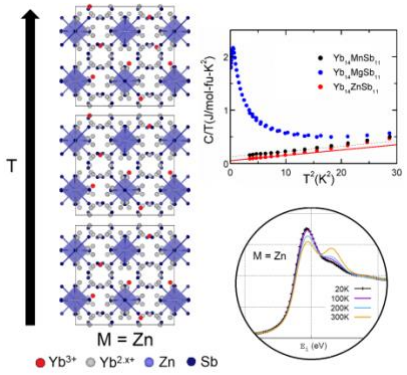

Keywords: thermoelectrics, XANES, Kondo effect, intermediate valence, magnetism

Allan He, Elizabeth L. Kunz Wille, Liane M. Moreau, Sean M. Thomas, Jon M. Lawrence, Eric D. Bauer, Corwin H. Booth, Susan M. Kauzlarich**

Intermediate Yb Valence in the Zintl Phases $Yb_{14}MSb_{11}$ (M = Zn, Mn, Mg): XANES, Magnetism, and Heat Capacity